Journal of Power Sources 196 (2011) 2164–2170

Contents lists available at ScienceDirect

Journal of Power Sources

journal homepage: www.elsevier.com/locate/jpowsour

Iron oxide porous nanorods with different textural properties and surface composition: Preparation, characterization and electrochemical lithium storage capabilities

Pedro Tartaj*, Jose M. Amarilla**

Instituto de Ciencia de Materiales de Madrid (CSIC), Campus Universitario de Cantoblanco, 28049, Madrid, Spain

ARTICLE INFO

Article history:
Received 12 May 2010
Received in revised form
22 September 2010
Accepted 30 September 2010
Available online 8 October 2010

Keywords:
Iron oxide
Nanorods
Anodes
Porous materials
Self-assembly
Batteries

ABSTRACT

We here report a method for the facile and large scale preparation of lithium-ion battery anodes based on α-Fe_2O_3 (hematite) nanorods with different textural characteristics and surface composition. The method combines electrostatically driven self-assembly approaches with specific adsorption and magnetically easy to disrupt soft aggregates. Special emphasis has been set to correlate the textural characteristics (porosity) and surface composition (core, core–nanoshell and core–double nanoshells) of nanorods with their electrochemical response. Thus, we have shown that nanorods present a nanophase whose specific capacity strongly depends on the lithium transport distances (nanorods with slit-shape mesopores running along their long axis vs. non-porous or surface blocked nanorods). We have also shown that the capacity retention of this nanophase after several charge–discharge processes depends on maintaining the structural integrity of the nanorods. Essential for the success of this latter study has been the use of nanorods that offer a simple tool (oriented X-ray line broadening) to follow their electrochemical grinding. Our data suggest that α-Fe_2O_3 mesoporous nanorods could both operate at a voltage and retain a capacity similar to that of nanostructured lithium titanates anodes if actions are taken to prevent electrochemical grinding.

1. Introduction

The development of next-generation lithium ion batteries is a key to the success of electric and hybrid electric vehicles, next generation electronic devices and implantable medical devices [1–4]. Ideal batteries should be inexpensive, have high energy density, and be made from environmentally friendly materials. Iron oxide is one of the main components of the earth's crust which explains the interest in developing Li-ion batteries anodes based on hematite (α-Fe_2O_3) [2,5–15]. Reports on the electrochemical reduction of α-Fe_2O_3 with metallic Li to give metallic Fe date back to the earlier 1980s [16–18]. It is not, however, up to the pioneering work of Tarascon and co-workers in the year 2000 on the reversible full reduction of 3d-metal oxides that the research on α-Fe_2O_3 electrodes was not reignited [19]. So far most of the studies on α-Fe_2O_3 anodes have been focused in producing anodes with high capacity. Excluding some works that report capacity retention at 200 cycles of about 1300 mAh g^{-1} which comes to a surprise given that the theoretical capacity is 1007 mAh g^{-1} for full reduction (1300 mAh g^{-1} would involve both a significant and highly reversible contribution from the electrolyte) [15], a fundamental drawback of α-Fe_2O_3 anodes is the rapid loss of capacity during the first cycles when operating at voltages able to fully reduce them to metallic iron [6,7,12,13].

Our interest, thus, in α-Fe_2O_3 anodes is not based on its full reduction to give metallic iron but rather in recent results reported by Tarascon and co-workers on nanoscale effects observed in α-Fe_2O_3 anodes [6,7]. These authors clearly showed that α-Fe_2O_3 nanocrystals (20 nm) prepared by hydrothermal methods unlike micron-sized particles give phases that although only inserted 0.6 Li/α-Fe_2O_3 (100 mAh g^{-1}) could theoretically insert up to 1 Li/α-Fe_2O_3 (170 mAh g^{-1}) at a relatively high operating voltage (1.6 V vs. Li/Li^+) [6,7]. This relatively high operating voltage though it reduces the specific energy of the device could make these anodes intrinsically safer compared to graphite, which has an operating voltage close to Li electroplating potential and thus raises concerns over its safety [20]. In fact, both the operating voltage and theoretical capacity of this α-$Li_xFe_2O_3$ nanophase is similar to that of another very promising anode (nanosized Li titanates). These lithium titanate spinels operate at voltages about 1.4–1.6 V and have a theoretical capacity of 175 mAh g^{-1}.

* Corresponding author. Tel.: +34 913348984; fax: +34 913720623.
** Corresponding author. Tel.: +34 913349074; fax: +34 913349074.
E-mail addresses: ptartaj@icmm.csic.es (P. Tartaj), amarilla@icmm.csic.es (J.M. Amarilla).

0378-7753/$ – see front matter © 2010 Elsevier B.V. All rights reserved.
doi:10.1016/j.jpowsour.2010.09.116

As above-mentioned a problem found in α-Fe_2O_3 nanocrystals (20 nm) prepared by hydrothermal methods is that only insert up to 0.6 Li/α-Fe_2O_3 (0.5 Li after about 10 cycles at C/5 (1 Li/5 h)) [6,7]. The existence of a gradient in the lithium concentration within the particles is the basis for the reduction in Li uptake of α-Fe_2O_3 nanocrystals [7]. The outer part of the particles would be locally the richest in lithium and their inner part would consist in non-reacted hematite or with very low lithium concentration. Thus, it seems reasonable to suppose that particles with a relatively open structure could favor the electrochemical reaction of α-Fe_2O_3 with lithium resulting in an uptake close to the theoretical one for all the particle volume. Following this simple idea, we here report the facile and large scale preparation of α-Fe_2O_3 (hematite) nanorods with different textural characteristics (porous and non-porous nanorods) and surface composition (core, core–shell and core–double shell), and analyze their electrochemical response when used as anodes in lithium ion batteries. Specifically, we have mainly focused for analogy with the lithium titanate electrodes in achieving insertion capacities of 1 Li/α-Fe_2O_3 (170 mAh g^{-1}) at similar operating voltages (1.4–1.6 V vs. Li/Li^+). We have selected silica and zirconia (inner)-silica (outer) oxides as nanoshells for the core–shell and core–double shell nanorods, respectively. These two oxides are well-known insulator materials that could help us to study the influence of structural integrity on the electrochemical response of α-Fe_2O_3 nanorods.

2. Experimental

2.1. Preparation of goethite precursors

Uniform goethite nanorods were obtained by the aerial oxidation of $FeSO_4$ following a method described earlier [21]. The method consists in the aerial oxidation of $FeSO_4$ aqueous solutions with Na_2CO_3 at 40 °C ([$FeSO_4$] = 0.075 mol L^{-1}, [Na_2CO_3] = 0.45 mol L^{-1}, air-flow rate = (2 dm^3 min^{-1}) and reaction time = 3 h). The method allows the large scale production of uniform nanorods in water at relatively low temperatures (40 °C) and atmospheric pressure. An additional advantage of the method not explored here is that the size of the nanorods can be modified by changing the Fe (II) salt and carbonate concentration, the air-flow rate and the reaction time.

2.2. Silica coated goethite precursors

Goethite is highly dispersible in water media at both acid and basic pH (isoelectric point of our goethite samples is about 8–9). Its high dispersability have allowed us to develop a method based on electrostatically driven self-assembly combined with specific adsorption to coat in a single experiment with a large amount of goethite per volume of water (5 g L^{-1}) with a large amount of silica (35 wt%). A silica content of 35% corresponds to a coating layer of about 5–10 nm for the α-Fe_2O_3 nanorods having sizes of 90 × 25 nm (as the ones described in the main text of the article). The success of this methodology lies on working in conditions close to a secondary minimum (as defined by the DLVO, Derjaguin–Landau–Vervey–Oberbeek, theory) in which aggregates are easily disrupted by stirring. The methodology consists first in reversing the charge surface of goethite from a negative to a positive value at a pH of 12. We need to do this change for adsorbing the negatively charged silicate species onto goethite surface and to start from a pH in which the silicate species are still in solution. To reach this goal we adsorb at a pH of 12 a cationic polyelectrolyte (poly(diallyldimethylammonium chloride), PDDA) which is typically used in layer-by-layer electrostatic approaches [22]. The PDDA concentration was set to 10^{-5} M. After adsorption, the sample was centrifuged and washed twice with water. Experimental evidence of the polyelectrolyte adsorption was achieved by electrophoretic mobility measurements. Then, a suspension of this material containing 5 g L^{-1} was prepared and brought to a pH of 12 using an ultrasound. This suspension was then transferred to a magnetic stirrer where KNO_3 (up to 0.25 M) was slowly added. After 30 min under strong magnetic stirring the necessary volume of a solution of Na_2SiO_3 (0.1 M, pH = 14) was added to give a final silica content of 35%. After 30 min under strong magnetic stirring the pH was lowered with HNO_3 to 11.3 and the suspension was again kept under strong magnetic stirring other 30 min. After that, CO_2 was bubbled into the suspension to lower the pH slowly. Under these conditions we assure that the suspension is close to a secondary minimum when lowering the pH with the CO_2. To generate the CO_2 we used a $NaHCO_3$ saturated solution (1 M) bubbled at air-flow rate of 2 dm^3 min^{-1}. The experiment was stopped after 15 h (pH of the suspension was 8.9) and the solids were centrifuged and washed several times. At pH between 12 (starting point) and 9 (ending point) silicate species are easily adsorbed onto the positively charge surface of the PDDA–goethite.

2.3. Goethite nanorods coated with a zirconia inner-shell and a silica outer-shell

The double shell consisted in an inner zirconia shell (10 wt%) and an outer shell composed of silica (25 wt%). The total concentration was set to a value of 35 wt% to match the amount of silica for the core–single shell coating. Our approach to efficiently deposit zirconia onto the surface of the goethite nanorods follows also a model that combines the electrostatically driven adsorption induced by cationic or anionic polyelectrolytes with the widely known capabilities of iron oxides to specifically adsorb cationic species in geological environments. Thus, goethite suspensions were ultrasonically dispersed in a water solution at a pH of 4. At a pH of 4 the goethite surface is positively charged and the anionic polyelectrolyte (poly(sodium 4-styrenesulfonate), PSS) was easily adsorbed. Polyelectrolyte layers were restricted to only one layer instead the normally used three or five layers to favor specific adsorption by the goethite substrate on pH zones where repulsive electrostatic interactions were dominant. Polyelectrolyte deposition was performed in magnetically stirred goethite suspensions (5 g L^{-1}) at a pH of 4 and then washed three times. The PSS concentration was set to a value of 10^{-3} M. Experimental evidence of the polyelectrolyte adsorption was achieved by electrophoretic mobility measurements. After washing, the negatively charged PSS-FeOOH nanorods were ultrasonically dispersed for 1 h at a pH of 3 and then the necessary amount of $ZrOCl_2$ was added to the dispersion. Then, the magnetically stirred dispersion containing the dissolved ZrO^{2+} species was slowly titrated with KOH 0.5 M until reach a pH of 4.5 (30 min of titration). The dispersion was kept at a pH of 4 for 1 h (using KOH 0.5 M). By using this methodology we assure the complete precipitation of the positively charged Zr oxyhydroxide compounds onto the negatively charged PSS-FeOOH nanorods. After deposition all samples were washed several times and dried in an oven at 50 °C. For the outer silica coating we followed a similar methodology to that carried out for the silica deposition into the goethite nanorods. Thus, we first turned the charge surface of the zirconia coated goethite nanorods at a pH of 12 to a positive value by adsorption of PDDA. Then, a suspension of this material was transferred to a magnetic stirrer where KNO_3 (up to 0.25 M) was slowly added. Then, the necessary volume of a solution of Na_2SiO_3 (0.1 M, pH = 14) was added to give a final silica content of 25% and the pH was slowly lowered down to a pH of 9 by bubbling CO_2.

2.4. Thermal treatment and selective dissolution of the silica layer

Silica coated α-Fe_2O_3 nanorods were obtained after heating the silica coated goethite nanorods at 400 for 2 h. Silica–zirconia α-Fe_2O_3 nanorods were obtained after heating the silica–zirconia coated goethite nanorods at 400 for 2 h. Porous bare α-Fe_2O_3 nanorods were obtained after heating the silica coated goethite nanorods samples at 400 for 2 h and further removing of the silica layer by stirring for 24 h KOH 2 M water suspensions of the material. Non-porous bare α-Fe_2O_3 nanorods were obtained after heating the silica coated goethite nanorods samples at 700 for 2 h and further removing of the silica layer by stirring for 24 h KOH 2 M water suspensions of the material.

2.5. Sample characterization

Morphology, particle size and EDX analyses of the obtained samples were carried out with a TEM JEOL microscope working at 200 keV. The mean size (X) and the standard deviation (SD) were evaluated from the electron micrographs by counting 100 particles. Phase identification was performed by X-ray analysis. X-ray diffraction (XRD) patterns were collected from 5° to 70° (2θ) by using a Bruker D8 Advance instrument with Cu Kα radiation ($\lambda = 0.15406$ nm) equipped with a SOLX detector that efficiently discriminates fluorescence. The instrument was operated at 40 kV and 30 mA. Nitrogen adsorption and desorption isotherms were performed at −196 °C in a Micromeritics ASAP 2010 volumetric adsorption system. The BET surface area was deduced from the analysis of the isotherm in the relative pressure range from 0.04 to 0.20. Pore size distributions were estimated using the BJH model. Electrophoretic mobility measurements were carried out in a Zetasizer nano (MALVERN). The study of the electrochemical properties of the α-Fe_2O_3 nanorods was performed in a two-electrode Li-cells. Positive electrode composites containing ≈10 mg of α-Fe_2O_3 (40 wt%), MMM Super P carbon black (40 wt%), and polyvinylidenedifluorine (PVDF, 20 wt%) were made by stirring for 3 h the powders in N-methylpyrrolidinone as fugitive solvent. The solvent was evaporated at 80 °C, and cylindrical pellets (12 mm diameter and ≈0.2 mm thickness) of positive electrode were obtained after cold pressing at 370 MPa. The pellets were stored at 80 °C. The negative electrode was a lithium foil, which also operated as reference electrode. The electrodes were separated by a Whatman BSF80 paper soaked in the electrolyte, which was a 1 M solution of $LiPF_6$ in ethylene carbonate and dimethyl carbonate (1:1 by volume) as supplied by UBE Europe GmbH. The components were assembled into a Swagelok® cell within an argon glove box in which water content was kept below 1 ppm. The cell was galvanostatically cycled at room temperature in different voltage ranges at 220 mA g^{-1} with an Arbin battery tester system (BT4 Model).

3. Results and discussion

3.1. Fundaments of the synthetic route used for the preparation of iron oxide porous nanorods with different textural properties and surface composition

Fig. 1 shows a schematic representation of the methodology used to prepare hematite nanorods with different textural characteristics (porous and non-porous) and surface composition (core–shell and core–double shell nanorods). Our approach for the facile and large scale preparation of these nanorods is basically based on the use of goethite (α-FeOOH) as solid precursor of α-Fe_2O_3 nanorods. A look to the well-known $Fe/O_2/H_2O$ system let us to anticipate that goethite could be the ideal solid precursor to easily obtain α-Fe_2O_3 nanorods with different textural characteristics. Methods based on a modified carbonate route (see Section 2 for details) have been used for the large scale production of monodisperse goethite nanorods [21,23–26]. In fact, goethite is one of the main components in the lateritic soils found in the tropical and subtropical regions of Cuba, Brazil, The Philippines, Indonesia and southern China [27,28].

Goethite naturally adopts an elongated morphology which run parallel to the [0 0 1] direction. On heating a goethite crystal transforms into a mosaic of highly oriented hematite crystal (<5 nm across) separated by pairs of slit-shaped micropores (0.8 nm wide) running along the goethite long axis (porosity is the direct

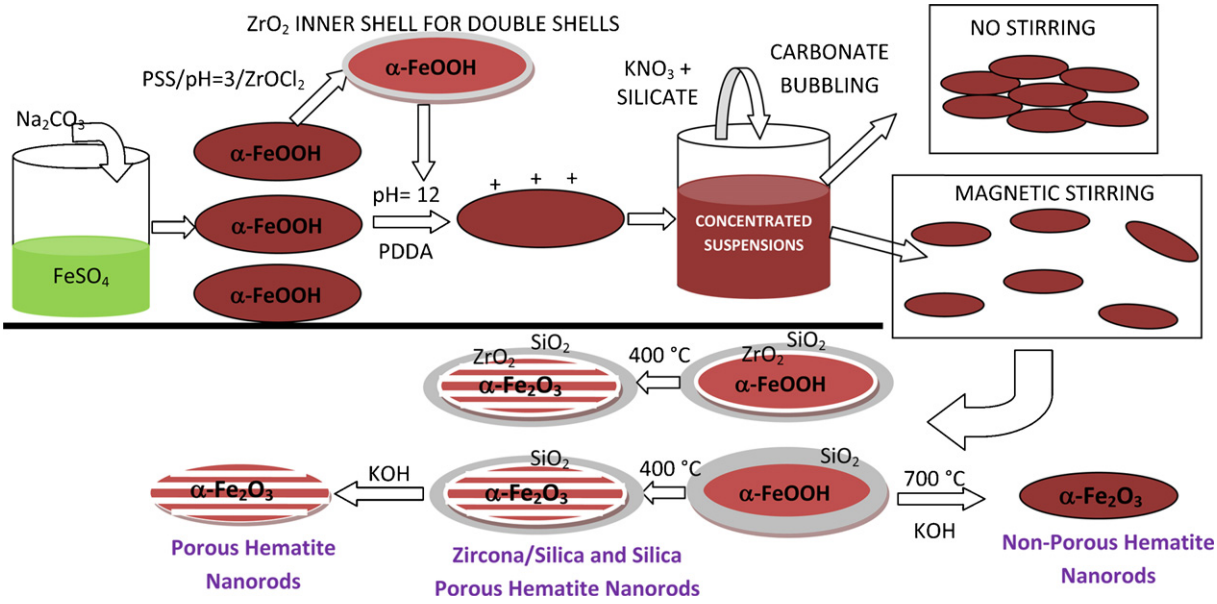

Fig. 1. Schematic representation of the experimental route carried out to obtain porous and non-porous α-Fe_2O_3 (hematite) nanorods as well as silica and zirconia–silica coated α-Fe_2O_3 porous nanorods. Basically a modified carbonate route has been used for the large scale production of monodisperse α-FeOOH (goethite) nanorods. Then a method that combines the electrostatically driven self-assembly with specific adsorption and magnetically easy to disrupt soft aggregates allows the large scale coating of α-FeOOH nanorods. Finally, thermal heating is applied to produce the coated α-Fe_2O_3 porous (400 °C) and non-porous (700 °C) nanorods. Bare porous or non-porous α-Fe_2O_3 nanorods are obtained by removing in basic media the silica coating of the silica α-Fe_2O_3 coated nanorods.

consequence of dehydroxilation). On continued heating hematite crystallites grow by a surface diffusion/coalescence process and the micropores are converted into mesopores to finally disappear at temperatures above 600–700 °C [29]. Furthermore goethite seems also a suitable material to easily obtain core–shell α-Fe_2O_3 nanorods. On one hand goethite is widely reported to have unique capabilities to specifically adsorb cationic species in geological environments [30]. On the other hand, relatively concentrated colloidal aqueous suspensions of goethite can be easily prepared. These two properties indicate that a method based on the electrostatically driven adsorption induced by cationic or anionic polyelectrolytes could be developed for the large scale production of core–shell structures. Specifically by working in conditions close to a secondary minimum (as defined in the DLVO theory, Derjaguin–Landau–Vervey–Oberbeek) in which aggregates are easily disrupted by stirring, we have been able to coat in a single experiment a large amount of material onto a large amount of nanorods (see Section 2 for details).

A drawback of the method is that interparticle sintering takes place simultaneously to pore coalescence and disappearing. Thus, to preserve the rod-like morphology during the heating that leads to porous α-Fe_2O_3, a protecting layer must be deposited onto the surface of goethite. However, this drawback does not suppose a significant inconvenient because the method developed for the efficient deposition of a nanoshell allows us also to efficiently deposit suitable coatings to prevent interparticle sintering during heating (see Section 2 for details). For example, silica that can be easily dissolved in basic media after heating seems a suitable protective layer to obtain uncoated porous and non-porous nanorods. Silica nanoshells as we will see below also allow us to study the influence of structural integrity on the electrochemical response of α-Fe_2O_3 nanorods.

3.2. Crystallochemical, morphological and textural characteristics of α-Fe_2O_3 nanorods

Heating silica coated goethite precursors at temperatures of 400 °C/2 h followed by selective removing in basic media of the silica layer (see Section 2 for details) leads to α-Fe_2O_3 nanorods (90 × 25 nm) with slit-shaped mesostructured porosity centered about 5 nm and a BET surface area of 150 $m^2 g^{-1}$ (Figs. 2 and 3). Heating at 700 °C/12 h followed also by the selective removing of the silica coating (Figs. 2 and 3) leads to bare α-Fe_2O_3 nanorods with a significant reduction in both the pore population centered about 5 nm and the BET surface area (75 $m^2 g^{-1}$). Pore elimination in this sample causes also a significant volume contraction (75 × 15 nm). In fact, TEM pictures (Fig. 2) show that the slit-shaped pores running along the long axis have almost disappeared, which explains the more pronounced contraction for the short axis (40% vs. 15%). Fig. 4 (goethite heated at 400 °C/2 h with retention of the coating) clearly shows that the experimental method developed to deposit the nanoshells was indeed successful. Fig. 4 also shows the image of a sintered α-Fe_2O_3 sample (obtained from bare goethite heated at 900 °C/12 h plus 600 °C/24 h) that was prepared to compare its electrochemical response with that of the nanorods.

3.3. Electrochemical lithium storage capabilities of α-Fe_2O_3 nanorods

As mentioned in Section 1 our interest in α-Fe_2O_3 anodes is not based on its full reduction to give metallic iron but rather in recent results reported by Tarascon and co-workers on nanoscale effects observed in α-Fe_2O_3 anodes [6,7]. These authors clearly showed that α-Fe_2O_3 nanocrystals (20 nm) prepared by hydrothermal methods unlike micron-sized particles give phases that although

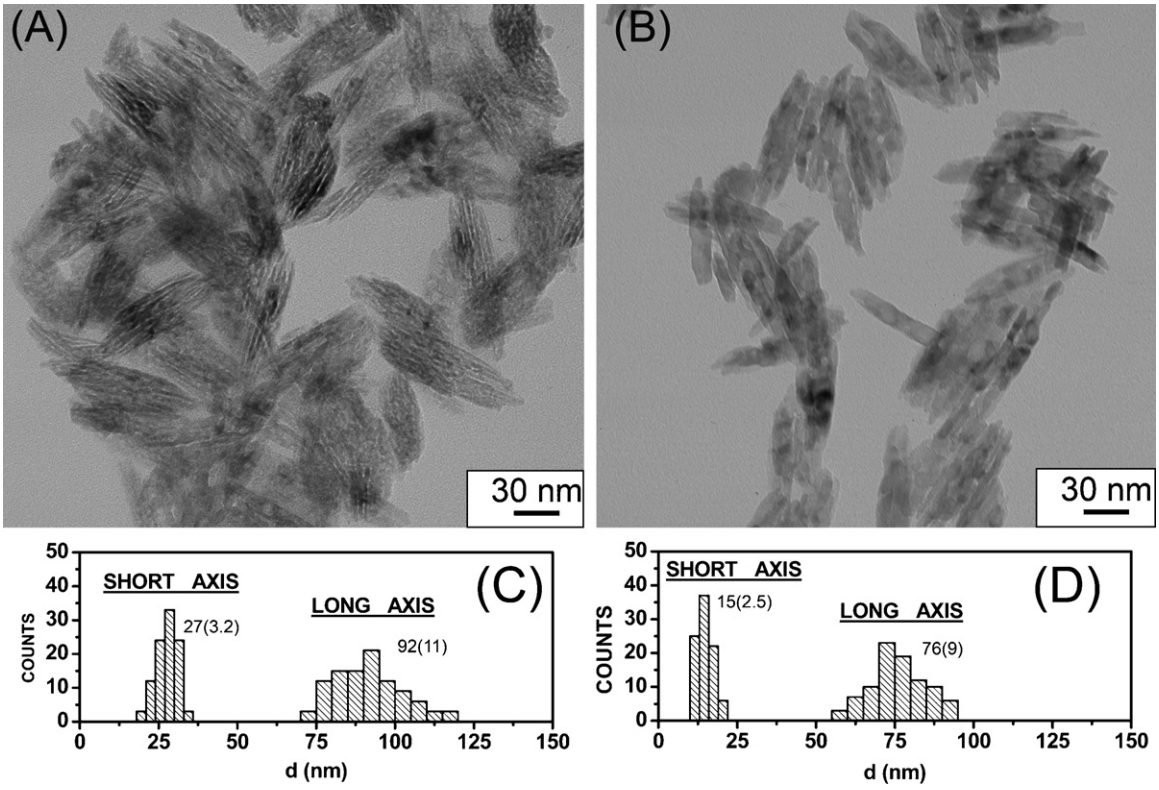

Fig. 2. TEM pictures of silica coated goethite solid precursors thermally treated at (A) 400 °C/2 h and (B) 700 °C/12 h followed by elimination of the silica coating in basic media. The scale bar is the same for the two TEM pictures. (C) Size distribution histograms and mean and standard deviation for the samples heated at 400 °C/2 h and (D) at 700 °C/12 h.

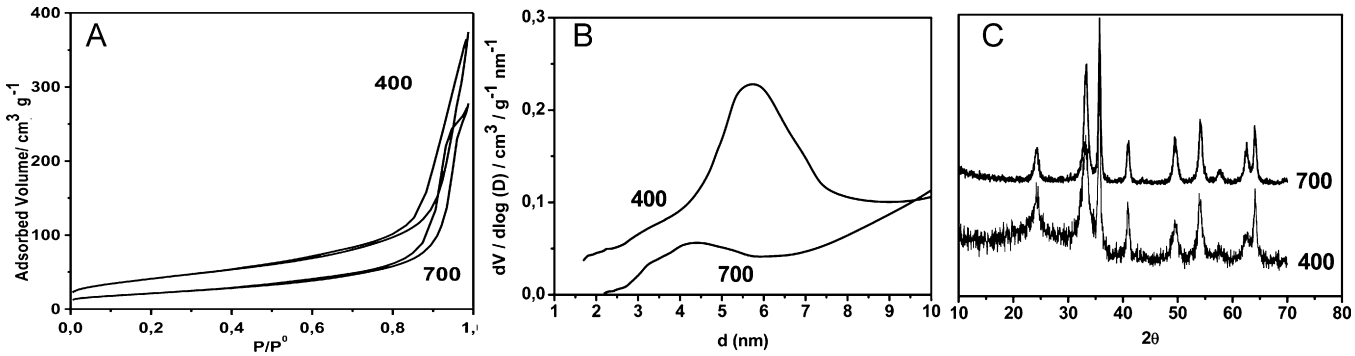

Fig. 3. (A) N_2 adsorption–desorption isotherms of silica coated goethite solid precursors thermally treated at 400 °C/2 h and 700 °C/12 h followed by elimination of the silica coating in basic media. (B) Pore size distributions calculated based on the BJH model for the samples heated at these temperatures. (C) X-ray diffraction (XRD) patterns for the two samples. The patterns only show diffraction peaks associated with α-Fe_2O_3. XRD clearly reveals broadening in directions that run parallel to the short axis of the nanorods which is less intense in the sample heated at 700 °C/12 h because pore coalescence and crystal growth occurs simultaneously.

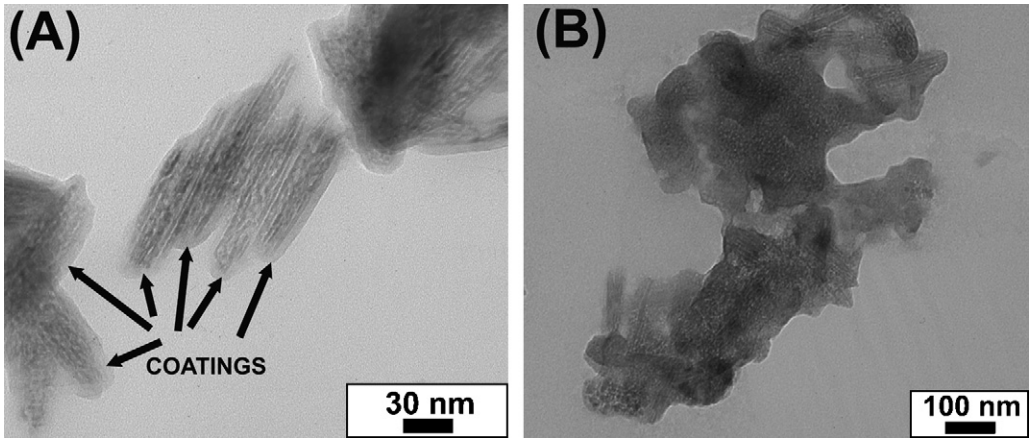

Fig. 4. (A) TEM picture for the silica coated goethite solid precursor thermally treated at 400 °C/2 h that clearly shows that the experimental method developed to deposit the nanoshells was indeed successful. The TEM picture for the zirconia/silica coated was similar. The presence of zirconia was noted by chemical analyses carried out by EDX in single particles. Zirconia is the inner shell and only represents a 10 wt% while the outer shell composed of silica represents a 25 wt% (35 wt% for the single shell case). In fact, the situation is even worse if one considers the density of both oxides (5 for zirconia vs. 2 g cm^{-3} for silica). Thus, it is rather normal not to clearly see the zirconia inner shell. (B) TEM picture obtained from bare goethite heated at 900 °C/12 h plus 600 °C/24 h. Note that the scale bar is significantly larger in (B).

only inserted 0.6 Li/α-Fe_2O_3 (100 mAh g^{-1}) could theoretically insert up to 1 Li/α-Fe_2O_3 (170 mAh g^{-1}) at a relatively high operating voltage (1.6 V vs. Li/Li^+) [6,7].

Prior to analyze the operating voltage region around 1.5 V some useful information can be extracted from the analysis of the first discharge curves down to full reduction (cutoff voltage 0.01 V) even though as above-mentioned this is a highly irreversible process [6,7,12,13]. The samples studied were bare α-Fe_2O_3 mesoporous (400 °C/2 h) and non-porous (700 °C/12 h) nanorods, silica coated and zirconia/silica α-Fe_2O_3 mesoporous nanorods (400 °C/2 h with retention of the coating) and sintered α-Fe_2O_3 (obtained from bare goethite heated at 900 °C/12 h plus 600 °C/24 h). The analysis of the first discharge curves (Fig. 5) show the presence of a long plateau at about 0.8 V which is due to the formation of a highly irreversible phase (cubic-$Li_2Fe_2O_3$) and the further reduction of this phase to give metallic Fe [6–8,12,13]. The capacity values associated with the reduction were in all cases high (1590 for porous, 1610 for non-porous, 1750 for silica-porous, 2080 for zirconia–silica-porous, and 1090 mAh g^{-1} for the sintered sample). These values correspond to 9.5, 9.6, 10.4, 12.4 and 6.5 Li per α-Fe_2O_3, respectively. In fact, based on a full reduction of Fe^{3+} to Fe^0, one would expect a maximum uptake of 6 Li/α-Fe_2O_3. The large excess in capacity for the nanorods can be regarded as originating from the low-voltage decomposition of the electrolyte. This decomposition is believed to occur below the 0.8 V region though nanoparticles (as it is the case of the nanorods here prepared) can catalyze such a decomposition at slightly higher potentials [6,7]. It is also worthy of noting that the silica and zirconia–silica coatings do not block the reduction of Fe^{3+} to Fe^0, that is, they do not completely block the electrochemical reaction with lithium.

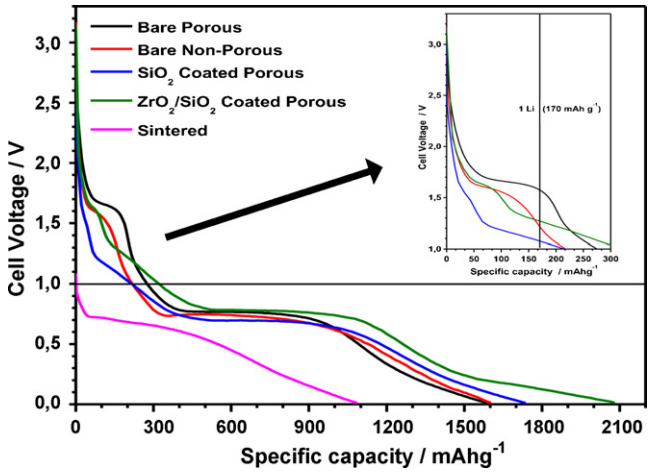

Fig. 5. First discharge curve of bare α-Fe_2O_3 porous nanorods, non-porous nanorods, silica and zirconia–silica coated α-Fe_2O_3 porous nanorods and sintered α-Fe_2O_3. Inset shows a zoom at operating voltages higher than 1.0 V (a line showing an uptake of 1 Li/α-Fe_2O_3 is marked).

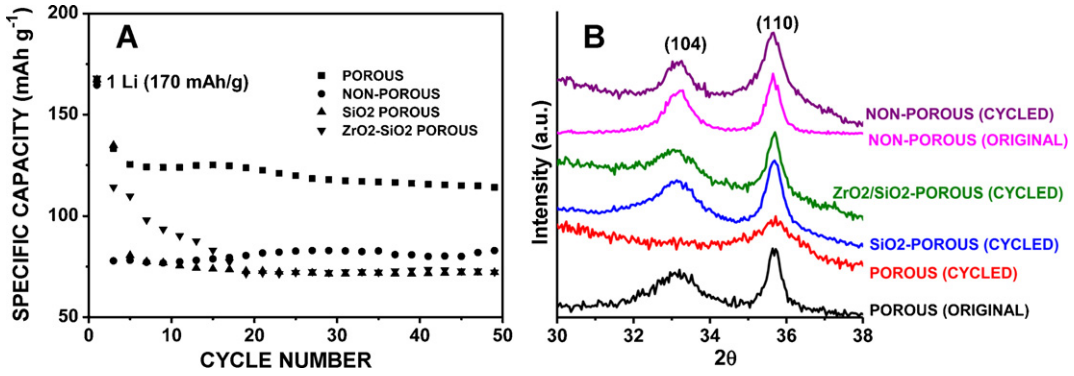

Fig. 6. (A) Cycling performance up to an uptake of 1 Li/α-Fe_2O_3 (170 mAh g^{-1}) of bare α-Fe_2O_3 porous nanorods, bare α-Fe_2O_3 non-porous nanorods and zirconia–silica and silica coated α-Fe_2O_3 porous nanorods. (B) X-ray diffraction patterns for the bare α-Fe_2O_3 porous nanorods, and zirconia–silica and silica coated α-Fe_2O_3 porous nanorods as well as for the non-porous after the cycling (an original sample has also been included for comparison). XRD clearly reveals broadening in the direction whose main component runs parallel to the short axis of the nanorod and a narrow peak in the direction whose main component runs parallel to the long axis. A significant broadening in the narrow peak (loss of rod-like morphology) is only observed for the bare α-Fe_2O_3 porous nanorods. This result is associated with electrochemical grinding.

We are, however, interested in the operating voltage region around 1.5 V (electrodes intrinsically safer). For example, in our samples as above mentioned nanorods catalyze the decomposition of the electrolyte at 0.8 V. As expected, the sintered sample does not show any significant electrochemical reaction until an operating voltage of about 0.8 V is reached. However, the nanorods clearly exhibit the signatures of electrochemical processes at operating voltages above 1 V. Thus, bare nanorods with slit-shaped mesoporosity clearly display a plateau region about 1.7 V which extends up to 1 Li/α-Fe_2O_3 (170 mAh g^{-1}) while the non-porous nanorods also exhibit a plateau region at this operating voltage but with a significant reduction in specific capacity (0.7 Li/α-Fe_2O_3). We, thus, could conclude that lithium transport distances play a significant role in the electrochemical processes that occur at operating voltages higher than 0.8 V. In fact, on the basis of an uptake of 1 Li/α-Fe_2O_3 for the non-porous nanorods we could think that the electrochemical reaction is retarded with respect to the porous nanorods because of longer lithium transport distances (i.e. shifted to a lower cell voltage, 1.2 V, Fig. 5). The cases of the porous nanorods in which the silica and zirconia–silica surface layers have been preserved are very helpful in this issue. Impedance effects associated with the presence of these insulating nanolayers clearly retard the electrochemical reaction shifting the operating voltage on the basis of an uptake of 1 Li/α-Fe_2O_3 at lower voltages when compared to the bare porous nanorods (1.1 V for silica and 1.3 V for the zirconia–silica coated nanorods). Thus, from this study we can conclude that during the first discharge process, bare nanorods with slit-shaped mesoporosity reach a capacity of 170 mAh g^{-1} at a relatively high operating voltage (1.7 V vs. Li/Li^+), that is, very similar to the behavior of Li nanosized titanates [31,32]. The picture, however, needs to be completed by studying the capacity retention after several charge–discharge processes. The cycling performance after 50 cycles of the nanosized materials up to an uptake of 1 Li/α-Fe_2O_3 (170 mAh g^{-1}) is displayed in Fig. 6A. Bare nanorods with slit-shaped mesoporosity suffer a gradual loss in capacity retention (0.7 Li, 115 mAh g^{-1}, at 1*C* after 50 cycles). On the other hand, the non-porous and the coated porous samples suffer a more pronounced loss of capacity during the first charge–discharge cycles reaching a constant value (80 mAh g^{-1}, 0.5 Li) after 20 cycles for the slower samples.

As above-mentioned previous studies on hematite particles of about 20 nm prepared by hydrothermal methods indicated that there was a limit for lithium uptake of about 0.6 Li/α-Fe_2O_3 (0.5 Li after about 10 cycles at only C/5) [6,7]. Furthermore, these studies also indicated that electrochemical grinding also took place in such small particles. Fig. 6B clearly shows the effect of electrochemical grinding in the bare nanorods. A significant broadening in the direction whose main component runs parallel to the long axis is only observed for the bare nanorods with slit-shape mesoporosity (i.e. loss of rod-like morphology). Our data, thus, suggest that the open structure of the bare nanorods having slit-shaped mesoporosity favors the electrochemical reaction with lithium. However, electrochemically driven grinding effects upon reaction with lithium could gradually damage the integrity of the bare porous nanorods making more difficult their electrochemical reaction with lithium. Thus, the final picture is that irreversibility processes associated with surface groups are gradually favored in the bare porous nanorods as the structural damage takes place, and capacity retention is gradually lost in the bare porous nanorods after each charge and discharge process. For the other samples here prepared (non-porous and coated) and the hematite particles of about 20 nm prepared by hydrothermal methods [6,7], the electrochemical reaction with lithium is already hindered from the beginning of the process and strong irreversibility associated with surface processes can take place rapidly. Finally, it should be mentioned that the bare nanorods with slit-shaped mesoporosity still show a capacity retention of about 0.7 Li (115 mAh g^{-1}) at 1*C* (1 Li/h) after 50 cycles. This capacity retention is significantly higher than the 0.5 Li after about 10 cycles at only C/5 (1 Li/5 h) for hydrothermally prepared 20 nm nanocrystals.

4. Conclusions

We have shown that a method that combines the electrostatically driven self-assembly with specific adsorption and magnetically easy to disrupt soft aggregates is adequate for the production of α-Fe_2O_3 (hematite) nanorods with different textural characteristics (porosity) and surface composition (core, core–nanoshell and core–double nanoshells). We have also shown that lithium-ion battery anodes based on the use of these nanorods present a phase whose specific capacity at safe operating voltages (~1.6 V) strongly depends on the textural characteristics of the nanorods. Thus, the specific capacity can be increased by a factor of about 1.5 when slit-shape mesopores running along the long axis of nanorods are present. This increase in capacity at relatively high operating voltages has been associated with the high accessibility for lithium that nanorods having slit-shaped mesoporosity do have. On the other hand, the gradual loss of capacity after several charge–discharge processes has been associated with electrochemical grinding. Thus, we anticipate that α-Fe_2O_3 mesoporous materials in which actions have been taken to prevent electrochemical grinding could operate at voltages and

retain a capacity similar to that of nanosized lithium titanate anodes.

Acknowledgments

We acknowledge financial support from the Spanish Ministerio de Ciencia e Innovacion through MAT2008-03224/NAN and MAT2008-03182.

References

[1] M. Armand, J.M. Tarascon, Nature 451 (2008) 652–657.
[2] J. Chen, F. Cheng, Acc. Chem. Res. 42 (2009) 713–723.
[3] C. Jiang, E. Hosono, H. Zhou, Nanotoday 1 (2006) 28–33.
[4] R. Ruffo, S.-S. Hong, C.K. Chan, R.A. Huggins, Y. Cui, J. Phys. Chem. C 113 (2009) 11390–11398.
[5] J. Sarradin, M. Ribes, A. Guessous, K. Elkacemi, Solid State Ionics 112 (1998) 35–40.
[6] D. Larcher, C. Masquelier, D. Bonnin, Y. Chabre, V. Masson, J.B. Leriche, J.M. Tarascon, J. Electrochem. Soc. 150 (2003) A133–A139.
[7] D. Larcher, D. Bonnin, R. Cortes, I. Rivals, L. Personnaz, J.M. Tarascon, J. Electrochem. Soc. 150 (2003) A1643–A1650.
[8] A.S. Arico, P. Bruce, B. Scrosati, J.M. Tarascon, W. Van Schalkwijk, Nat. Mater. 4 (2005) 366–377.
[9] J. Chen, L. Xu, W. Li, X. Gou, Adv. Mater. 17 (2005) 582–585.
[10] H. Morimoto, S. Tobishima, Y. Iizuka, J. Power Sources 146 (2005) 315–318.
[11] J. Morales, L. Sanchez, F. Martin, F. Berry, X. Ren, J. Electrochem. Soc. 152 (2005) A1748–A1754.
[12] C. Wu, P. Yin, X. Zhu, C.-O. Yang, Y. Xie, J. Phys. Chem. B 110 (2006) 17806–17812.
[13] X.-L. Wu, Y.-G. Guo, L.-J. Wan, C.-W. Hu, J. Phys. Chem. C 112 (2008) 16824–16829.
[14] J. Li, H.M. Dahn, L.J. Krause, D.-B. Le, J.R. Dahn, J. Electrochem. Soc. 155 (2008) A812–A816.
[15] P.C. Wang, H.P. Ding, T. Bark, C.H. Chen, Electrochim. Acta 52 (2007) 6650–6655.
[16] M.M. Thackeray, J. Coetzer, Mater. Res. Bull. 16 (1981) 591–597.
[17] B. Di Pietro, M. Matriarca, B. Scrosati, J. Power Sources 8 (1982) 289–299.
[18] M.M. Thackeray, W.I.F. David, J.B. Goodenough, Mater. Res. Bull. 17 (1982) 785–793.
[19] P. Poizot, S. Laruelle, S. Grugeon, L. Dupont, J.M. Tarascon, Nature 407 (2000) 496–499.
[20] Y. Zhenguo, D. Choi, S. Kerisit, K.M. Rosso, D. Wang, J. Zhang, G. Graff, J. Liu, J. Power Sources 192 (2009) 588–598.
[21] R. Pozas, M.P. Morales, C.J. Serna, M. Ocana, J. Colloid Interface Sci. 254 (2002) 87–94.
[22] F. Caruso, Adv. Mater. 13 (2001) 11–22.
[23] N.O. Nunez, M.P. Morales, P. Tartaj, C.J. Serna, J. Mater. Chem. 10 (2000) 2561–2565.
[24] N.O. Nunez, R. Pozas, M.P. Morales, P. Tartaj, P. Bonville, A.R. Gonzalez-Elipe, A. Caballero, M. Ocana, C.J. Serna, Chem. Mater. 15 (2003) 951–957.
[25] N.O. Nunez, P. Tartaj, M.P. Morales, R. Pozas, M. Ocana, C.J. Serna, Chem. Mater. 15 (2003) 3558–3563.
[26] A.F. Rebolledo, O. Bomatí-Miguel, J.F. Marco, P. Tartaj, Adv. Mater. 20 (2008) 1760–1765.
[27] E. Ramanaidou, D. Nahon, A. Decarreau, J. Melfi, Clays Clay Miner. 44 (1996) 22–31.
[28] P. Tartaj, A. Cerpa, M.T. Garcia-Gonzalez, C.J. Serna, Clays Clay Miner. 50 (2002) 342–347.
[29] R.M. Cornell, U. Schwertmann, in: VCH (Ed.), The Iron Oxides: Structure, Properties, Reactions and Uses, VCH, Weinheim, 1996.
[30] A.S. Madden, M.F.A. Hochella Jr., Geochim. Cosmochim. Acta 69 (2005) 389–398.
[31] L. Kavan, M. Gratzel, Electrochem. Solid State Lett. 5 (2002) A39–A42.
[32] J. Kim, J. Cho, Electrochem. Solid State Lett. 10 (2007) A81–A84.